Image-Based Trajectory Tracking Control of 4-DoF Laparoscopic Instruments Using a Rotation Distinguishing Marker

Zerui Wang, *Student Member, IEEE*, Sing Chun Lee, Fangxun Zhong, *Student Member, IEEE*, David Navarro-Alarcon, *Member, IEEE*, Yun-hui Liu, *Fellow, IEEE*, Anton Deguet, Peter Kazanzides, *Member, IEEE*, and Russell H. Taylor, *Life Fellow, IEEE*

***Abstract*—In this letter, we propose a new method to fully control complete 4-image-DoF manipulation of laparoscopic instruments [with remote center of motion (RCM) mechanism] based on the geometric features of a designed marker in a 2-D image. Our marker encodes the configuration of the instruments by computing geometric features among the projected image points from segmented areas in hue-saturation-value (HSV) space. We can then construct an image geometric feature vector to locally characterize the configuration of a laparoscopic instrument. Furthermore, we design an image-based kinematic controller to asymptotically track a planned trajectory using the constructed feature vector as the feedback. We evaluate our integration of rotation distinguishing marker and kinematic controller by several experiments in terms of illumination-invariance, rotation angle accuracy, and controller performance.**

***Index Terms*—Surgical robotics, visual servoing.**

I. Introduction

NOWADAYS, minimally invasive approaches are used for many kinds of surgical procedures due to their significant benefit over conventional methods [1]. For example, laparoscopic surgery requires small abdominal incisions, which reduces the exposure of internal organs and prevents undue blood loss, thus shortens the recovery time and hospital stay [2]. However, it also brings challenges to laparoscopic surgeons. Limited work-space, restricted movements, and image-guided operations increase the difficulty of the surgical tasks, for which surgeon trainees need a longer training period to become proficient in comparison to conventional methods [3]. By contrast, the robots are more capable of working in this unfriendly imaging environment than human surgeons [4], which brings automated robotic surgery into consideration.

The mechanical [5] or virtual [6] remote center of motion (RCM) is widely adopted in surgical robots since it guarantees the safety by kinematic constraints at the entry point. The robots constrained by the RCM mechanisms only have angular reorientation about the RCM and translation that passes through the RCM. In most applications, surgeons control the instruments to a desired pose by manually sending the commands through an interface (e.g., a joystick, a control console) based on the laparoscopic image feedback of the scene inside the patient's body abdominal cavity (see [7], [8]). Since the laparoscope is the only image sensor, visual servoing integrated with low-level positioning servo loop becomes an intuitive control scheme for automated robotic surgery [9].

There are some works in the literature addressing image based automatic control for laparoscopic instruments. In [10], Azizian *et al.* provided a survey of the visual servoing applications in medical robotics. Bourger *et al.* used a combination of extended efficient second-order minimization (ESM) tracking algorithm and a histogram-based color feature comparison to track the region of interest even if parts of the view are occluded; a specific control strategy was developed to perform the ESM tracking with the AESOP robot [11]. Uecker *et al.* demonstrated vision-based aiming of a laparoscope held by an AESOP robot [12]. A four-step iteration algorithm was developed for instrument localization and tracking. Wei *et al.* proposed a visual tracking method for stereo laparoscopes using color information in HSV space for segmentation to track the instrument in both lateral and longitudinal motions [13]. Krupa *et al.*, in [14], proposed a method, which avoids the tool rotation, to localize the instrument with respect to the laparoscope scene by projecting laser patterns on the surface of the organs. Kim *et al.* presented a two-stage adaptive condensation algorithm to detect the tool tip position for real-time visual servoing of laparoscopic surgery [15]. Voros *et al.* reported the ViKY robotic scope holder which is a lightweight, sterilizable body-mounted robot and proposed a method to detect and track the instrument based on the image

Manuscript received September 8, 2016; accepted February 7, 2017. Date of publication March 1, 2017; date of current version March 29, 2017. This letter was recommended for publication by Associate Editor J. Hong and Editor K. Masamune upon evaluation of the reviewers comments. This work was supported in part by the HK RGC under Grants 415011 and CUHK6/CRF/13G, in part by the HK ITF Under Grants ITS/112/15FP and ITT/012/15GP, in part by the VC's Discretionary Fund through CURI under Grants 4930763 and 4930725, in part by the CUHK SHIAE under Grant 8115053, and in part by Johns Hopkins University Internal funds.

Z. Wang, F. Zhong, D. Navarro-Alarcon, and Y.-H. Liu are with the Department of Mechanical and Automation Engineering, The Chinese University of Hong Kong, Hong Kong (e-mail: zrwang@mae.cuhk.edu.hk; fxzhong@mae.cuhk.edu.hk; dnavarro@mae.cuhk.edu.hk; yhliu@mae.cuhk.edu.hk).

S. C. Lee, A. Deguet, P. Kazanzides, and R. H. Taylor are with the Department of Computer Science, Johns Hopkins University, Baltimore, MD 21218 USA (e-mail:singchun.lee@jhu.edu; anton.deguet@jhu.edu; pkaz@jhu.edu; rht@jhu.edu).

Digital Object Identifier 10.1109/LRA.2017.2676350

analysis and known instrument's shape [16]. Leven *et al.* used an optical marker with single spiral pattern attached on the ultrasound probe to compute the twist angle [17]. Stoll *et al.* used passive echogenic markers to determine the position and orientation of a surgical instrument in a 3-D ultrasound volume [18]. Taylor *et al.* developed a registration method for X-ray imaging using a corkscrew-like fiducial object mounted around the robot end-effector [19]. Zhao *et al.* invented a method to determine tool state by using the position and identification of the dotted pattern fiducial marker [20]. Most of these systems [12]–[16] can only track 3 degrees of freedom (DoF) of a laparoscopic instrument based on the camera image feedback. The tracking of the instrument's rotation is missed. However, this rotation angle is important for robotic automation since it determines the orientation of the instrument tip (e.g., dissector, grasper, forcep) which is essential to perform different surgical tasks such as dissection, in which the orientation should align with the expected dissection path.

Based on our previous work [21], in which we did position control for the 3-image-DoF configuration of an RCM mechanism using an uncalibrated camera, in this letter, we propose a new method to fully control complete 4-image-DoF manipulation of laparoscopic instruments (with RCM mechanism) based on the geometric features of a designed marker in a 2D image. The closest works to ours are [22] and [23]. Nageotte *et al.* proposed in [22] a method using four dotted markers distributed around the body of the needle-holder to get the rotation information of the instrument and expanded it in [23] to the path following of the instrument by an endoscope. In contrast, our marker encodes the configuration of the instruments by computing geometric features among the projected image points from segmented areas in Hue-Saturation-Value (HSV) space; these features allow us to independently control (locally) four image degrees of freedom of the instrument. We conduct several experiments to validate the proposed control method using a first generation da Vinci Surgical System with da Vinci Research Kit (dVRK) electronics [24]. The robot arm is mechanically constrained by an RCM. For a stable marker detection, we extract the marker features in HSV space for illumination-invariance, compute the features with cross-ratio for ratio-invariance in camera perspective space, and use area features instead of dots for robust pattern segmentation.

The rest of this manuscript is structured as follows: In Section II, we describe the mathematical models. Section III details the concept of the rotation distinguishing marker and the corresponding rotational angle computation algorithm. In Section V, we present the conducted experiments. Limitations and future improvements are discussed in Section VI.

II. Modeling

A. 4D Kinematics of Laparoscopic Instruments

The laparoscopic instrument we discuss in this letter has 4 DoFs: translation along its axis, rotation around its axis, left-right and forward-backward rotations around the incision point. Although many laparoscopic instruments (e.g., graspers, dissectors, forceps) have more degrees of freedom at the tool tips, it is still reasonable to study the basic problem without losing generality.

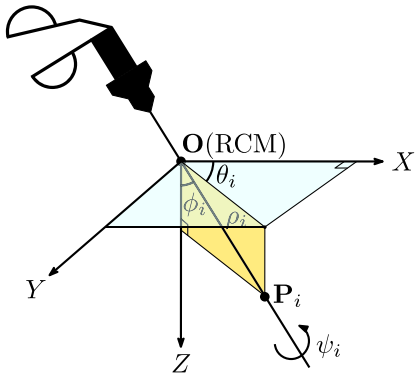

Fig. 1. The proposed extended spherical coordinate system. $\mathbf{P}_i$ is a point in Cartesian space, ρ_i is the insertion distance, θ_i and ϕ_i are the orientation angles, and ψ_i is the rotation angle.

Standard spherical coordinates can only define 3 DoF. Therefore, we extend it with an additional rotational DoF so as to fully define the configuration of a laparoscopic instrument. We set the origin of the coordinate system at the incision point (i.e. RCM). Let $\mathbf{q} \in \mathbb{R}^4$ be the extended coordinates which we define as

$$\mathbf{q} = \begin{bmatrix} \theta & \phi & \rho & \psi \end{bmatrix}^\intercal \tag{1}$$

where ρ is the insertion distance, ψ is the rotation angle and θ, ϕ are the orientation angles.

With (1), the Cartesian position $\mathbf{P}_i \in \mathbb{R}^3$ of any feature points located on the instrument can be described with spherical coordinates as follows (see Fig. 1)

$$\mathbf{P}_i = \rho_i \begin{bmatrix} \sin(\phi_i)\cos(\theta_i) & \sin(\phi_i)\sin(\theta_i) & \cos(\phi_i) \end{bmatrix}^\intercal \tag{2}$$

Note that the rotation of the instrument has no influence on the position of $\mathbf{P}_i$. Therefore, the rotation angle ψ_i does not appear in (2). Instead of using extended spherical coordinates $\mathbf{q}$, we use the image geometric vector $\mathfrak{f}$ defined in the image plane to locally parameterize the configuration of a laparoscopic instrument. Details can be found in Section II-D.

B. Perspective Projection of a Point

In reality, laparoscopic surgeons can only rely on the image feedback of a laparoscope to observe the situations inside the patient body. This feedback signal from the laparoscope is also the only sensor for the robot to position the instrument. In order to mimic the real surgical scenario, we consider an eye-to-hand set-up, in which a fixed monocular camera is placed near to the laparoscopic instrument to monitor its motion. We assume the camera is a pin-hole camera without distortion. Let vector $\mathbf{p}_i \in \mathbb{R}^2$ denote the projection of the feature point onto the image plane

$$\mathbf{p}_i = \begin{bmatrix} x_i & y_i \end{bmatrix}^\intercal \tag{3}$$

where the x_i and y_i are the pixel coordinates.

Under the perspective projection model [25]

$$\begin{bmatrix} \mathbf{p}_i \\ 1 \end{bmatrix} = \frac{1}{{}^c z_i} \mathbf{M} \begin{bmatrix} \mathbf{P}_i \\ 1 \end{bmatrix} \tag{4}$$

where the ${}^c z_i \in \mathbb{R}$ is the depth of the feature point with respect to the camera frame and $\mathbf{M} \in \mathbb{R}^{3\times 4}$ is the perspective projection matrix, which only depends on the camera's intrinsic and extrinsic parameters. Let $\mathbf{m}_i^\intercal$ denote the ith row vector of the perspective projection matrix $\mathbf{M}$. Then ${}^c z_i$ can be computed as follows

$${}^c z_i = \mathbf{m}_3^\intercal \begin{bmatrix} \mathbf{P}_i \\ 1 \end{bmatrix} \tag{5}$$

C. Remote Center of Motion (RCM)

Since the RCM of a laparoscopic instrument is always located at the incision point, the projection of RCM on the image plane is invisible and cannot be directly measured. In order to get the RCM's coordinates, we have to estimate them using feature projections in the image plane. Ideally, the projections of a laparoscopic instrument at different instants intersecting at the same point (RCM) in Cartesian space should also intersect at the same point on the image plane. However, due to coarse feature extraction results and machining errors, the above ideal case may not happen.

Let $\mathbf{l}_j \in \mathbb{R}^3$ denote the projection of the laparoscopic instrument at instant t_j

$$\mathbf{l}_j = \begin{bmatrix} a_j & b_j & c_j \end{bmatrix}^\intercal \tag{6}$$

where a_j, b_j and c_j are parameters of the homogeneous representation of 2D lines.

A line $\mathbf{l}_{jk}$ joining two points $\mathbf{p}_j$ and $\mathbf{p}_k$ is

$$\mathbf{l}_{jk} = \begin{bmatrix} \mathbf{p}_j \\ 1 \end{bmatrix} \times \begin{bmatrix} \mathbf{p}_k \\ 1 \end{bmatrix} \tag{7}$$

and two lines $\mathbf{l}_j$ and $\mathbf{l}_k$ intersecting at a point $\mathbf{p}_{jk}$ can be given as follows

$$\begin{bmatrix} \mathbf{p}_{jk} \\ 1 \end{bmatrix} = \frac{\mathbf{l}_j \times \mathbf{l}_k}{a_j b_k - a_k b_j} \tag{8}$$

At each time instance, we use the two points at two ends of the marker ($\mathbf{p}_{m_1}$ and $\mathbf{p}_{m_2}$, as shown in Fig. 2) to calculate the line (instrument projection) by (7). For N time instances, we could obtain N lines. Then, we calculate $M = C_N^2 = \frac{N(N-1)}{2}$ intersections among N lines by (8). Finally, the estimated projection of RCM $\hat{\mathbf{o}}$ could be obtained by taking the average of the intersection points by (9)

$$\hat{\mathbf{o}} = \frac{1}{M} \sum_{j=2}^{N} \sum_{k=1}^{j-1} \mathbf{p}_{jk} \tag{9}$$

The estimation differs from the real value by $\boldsymbol{\epsilon} = \hat{\mathbf{o}} - \mathbf{o}$. This error has no influence on the rotation angle estimation but affects the trajectory tracking. Details are in Sections II-D and III, respectively.

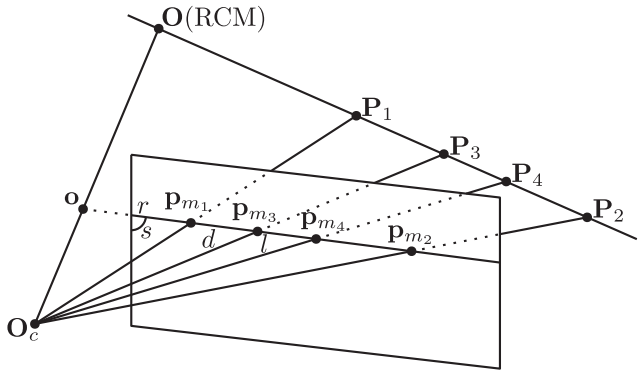

Fig. 2. An instrument with four feature points $\mathbf{P}_1, \mathbf{P}_2, \mathbf{P}_3$ and $\mathbf{P}_4$ on it and the constructed image features s, r, l and d using the point projections. $\mathbf{p}_{m_1}$, $\mathbf{p}_{m_2}$, $\mathbf{p}_{m_3}$, $\mathbf{p}_{m_4}$ and $\mathbf{o}$ are the perspective projection of the feature points and the RCM, respectively. $\mathbf{O}_c$ represents the optical center of a camera.

D. Image Geometric Features

To control the configuration of a laparoscopic instrument, we use the measurements of three image points, i.e., $\mathbf{p}_{m_1}$, $\mathbf{p}_{m_2}$ and $\mathbf{p}_{m_3}$ (see Fig. 2). We stack them into one extended image measurement vector $\mathfrak{p}_m \in \mathbb{R}^6$

$$\mathfrak{p}_m = \begin{bmatrix} \mathbf{p}_{m_1} & \mathbf{p}_{m_2} & \mathbf{p}_{m_3} \end{bmatrix}^\intercal \tag{10}$$

With $\mathfrak{p}_m$, we can construct an image geometric feature vector $\mathfrak{f}(\mathfrak{p}_m) \in \mathbb{R}^4$

$$\mathfrak{f}(\mathfrak{p}_m) = \begin{bmatrix} s(\cdot,\cdot) & r(\cdot) & l(\cdot,\cdot) & d(\cdot,\cdot) \end{bmatrix}^\intercal \tag{11}$$

to locally characterize the configuration of a laparoscopic instrument. Locally, we can parameterize the instrument extended spherical coordinates by the image geometric vector.

In (11), the scalar function $s(\mathbf{p}_{m_1}, \mathbf{p}_{m_2}) : \mathbb{R}^2 \times \mathbb{R}^2 \mapsto \mathbb{R}$ represents the angle between the instrument's projection and the vertical line (represented by the unit vector $\mathbf{e}_y$) in the image plane.

$$s(\mathbf{p}_{m_1}, \mathbf{p}_{m_2}) = \sin^{-1}\left(\frac{\|(\mathbf{p}_{m_2} - \mathbf{p}_{m_1}) \times \mathbf{e}_y\|}{\|\mathbf{p}_{m_2} - \mathbf{p}_{m_1}\|} \right) \tag{12}$$

The scalar function $r(\mathbf{p}_{m_1}) : \mathbb{R}^2 \mapsto \mathbb{R}$ represents the distance of the point $\mathbf{p}_{m_1}$ to the projection of RCM $\mathbf{o}$.

$$r(\mathbf{p}_{m_1}) = \|\mathbf{p}_{m_1} - \mathbf{o}\| \tag{13}$$

As shown in (13), r is a function with $\mathbf{o}$ as its parameter. Therefore, inaccurate estimation of $\mathbf{o}$ will affect the value of r. We will study how precise the estimation is in Section V-B.

The scalar function $l(\mathbf{p}_{m_1}, \mathbf{p}_{m_2}) : \mathbb{R}^2 \times \mathbb{R}^2 \mapsto \mathbb{R}$ represents the distance between the point $\mathbf{p}_{m_1}$ and the point $\mathbf{p}_{m_2}$.

$$l(\mathbf{p}_{m_1}, \mathbf{p}_{m_2}) = \|\mathbf{p}_{m_2} - \mathbf{p}_{m_1}\| \tag{14}$$

The scalar function $d(\mathbf{p}_{m_1}, \mathbf{p}_{m_3}) : \mathbb{R}^2 \times \mathbb{R}^2 \mapsto \mathbb{R}$ represents the distance between the point $\mathbf{p}_{m_1}$ and the point $\mathbf{p}_{m_3}$.

$$d(\mathbf{p}_{m_1}, \mathbf{p}_{m_3}) = \|\mathbf{p}_{m_3} - \mathbf{p}_{m_1}\| \tag{15}$$

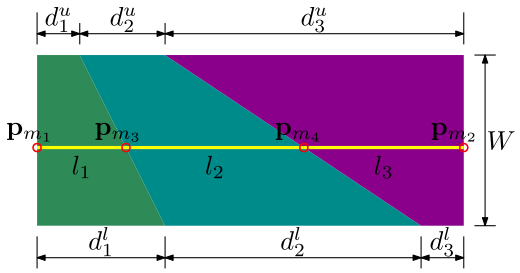

Fig. 3. The design of the rotation distinguishing marker. The yellow line represents the center of the marker's projection.

III. Rotation Distinguishing Marker

A. Design Criteria

Because one cannot observe rotation due to the homogeneous projected appearance from the cylindrical structure of the instrument, to visually obtain such feedback, we have designed an optical marker with the following criteria[1]:

1) Background distinguishable colors (e.g., distinguishable from abdominal cavity) for stable feature extraction;
2) Unique encoding of the rotation angle from the extracted geometric features;
3) Handling of geometric changes due to perspective projection.

Fig. 3 demonstrates a feasible marker design, which we used in our experiments.

B. Pattern Design

1) Area Feature and Color Scheme: To separate the markers from the background, we made use of the HSV space for avoiding using colors in the "red" zone. We picked three colors, whose hue values are 90, 180 and 270. The HSV space allows us the detect colors robustly invariant to the illumination changes [13]. It gives fast and stable marker segmentation results of the three selected colors. Furthermore, in comparison to dots features, which are typically used in optical markers, using areas is more robust for segmentation.

2) Intuitive Angle Encoding: To encode the rotation angles, areas are spread by the three colors with different patterns parameterized by the lengths $d_{\{1,2,3\}}^{\{u,l\}}$ as illustrated in Fig. 3. Intuitively, the horizontal length l_i (signified by $\mathbf{p}_{\mathbf{m}_i}$ and $\mathbf{p}_{\mathbf{m}_{i+1}}$ in Fig. 3) in the i-th area is able to encode the rotation angle ψ_i individually as follows:

$$\psi_i = \frac{2\pi(l_i - d_i^u)}{d_i^l - d_i^u} \tag{16}$$

The width W of the marker should equal to the circumference of the instrument plus the marker's thickness, so that after attaching the marker, the upper and lower edges are perfectly aligned and therefore (16) encodes 2π accurately.

[1]The marker is designed for recovering the rotation angle. It can be integrated with occlusion handling algorithms in [26].

Algorithm 1: Angle computing algorithm.

1: **for** each input image Img **do**
2: Segment the markers in HSV spaces into three areas $Area_i, i = 1, 2, 3$
3: Extract center line $Line$ from the combined result $Area = \cup_{i=1}^{3} Area_i$
4: Detect $\mathbf{p}_{\mathbf{m}_i}, i = 1, 2, 3, 4$ using the $Line$ and $Area_j, j = 1, 2, 3$, hence compute $\mathfrak{l}_i$
5: Compute cross-ratio $r(\mathfrak{l}_1, \mathfrak{l}_2, \mathfrak{l}_3)$ using (17)
6: Estimate the rotation angles ψ using (18)
7: **end for**

3) Perspective Space Preserved Area Encoding: However, to use (16), a precise length l_i in 3D is required. It is a challenging computer vision problem, particularly trying to measure it in 2D perspective space. Instead of solving this problem, we tackle the problem differently by taking advantage of the cross-ratio among the three measured horizontal lengths $\mathfrak{l}_i$ of the areas. Cross-ratio is defined as below:

$$r(l_1, l_2, l_3) = \frac{(l_1 + l_2)(l_2 + l_3)}{l_2(l_1 + l_2 + l_3)} \tag{17}$$

[27] proved that cross-ratio is preserved in perspective space. Therefore, the cross-ratio obtained directly in the 2D image is equivalent to the one obtained in parallel space as well as in 3D. Hence $r(l_1, l_2, l_3) = r(\mathfrak{l}_1, \mathfrak{l}_2, \mathfrak{l}_3)$. Furthermore, with the design in Fig. 3, the cross-ratio among l_i is linear and monotonic. Hence, we propose an encoding scheme of the rotation angle as follows:

$$\psi = \frac{2\pi(r - r^u)}{r^l - r^u} \tag{18}$$

where $r^u = r(d_1^u, d_2^u, d_3^u)$ and $r^l = r(d_1^l, d_2^l, d_3^l)$ by (17).

C. Algorithm

In summary, the algorithm is described in Algorithm 1.

IV. Controller Design

A. Trajectory Tracking Controller

Given the relationship defined in (2) and the estimated relative rotation angle, we can rewrite the image geometric feature vector $\mathfrak{f}(\mathfrak{p})$ in (11) with respect to extended coordinates, namely $\mathfrak{f}(\mathbf{q})$. Taking the time derivative yields

$$\dot{\mathfrak{f}}(\mathbf{q}) = \mathbf{J}\mathbf{v} \tag{19}$$

where $\mathbf{v} = \dot{\mathbf{q}} \in \mathbb{R}^4$ denotes the velocity control input, and $\mathbf{J} \in \mathbb{R}^{4\times4}$ denotes the Jacobian Matrix

$$\mathbf{J} = \frac{\partial \mathfrak{f}}{\partial \mathfrak{p}} \frac{\partial \mathfrak{p}}{\partial \mathbf{P}} \frac{\partial \mathbf{P}}{\partial \mathbf{q}} \tag{20}$$

Note that since the kinematics is different among different surgical robots, the above formulation does not include the mapping from extended coordinates to the robot joint space.

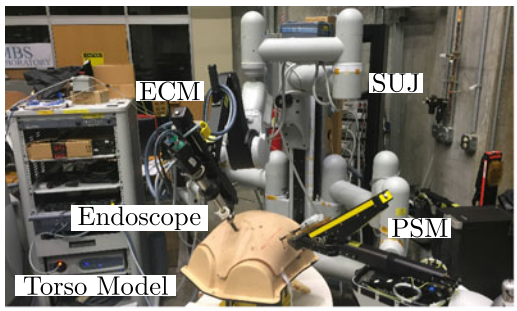

Fig. 4. The set-up of the experiments.

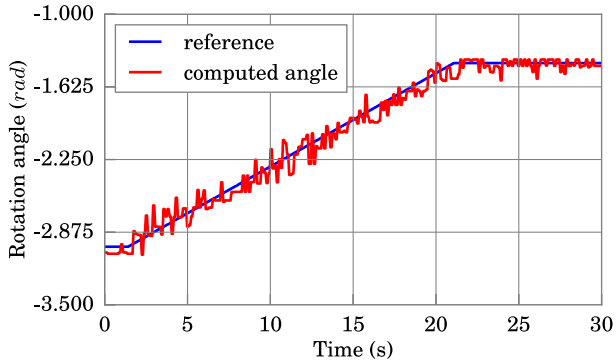

Fig. 5. The experimental result of the pure rotation experiment.

Problem statement: Design an image-based kinematic controller to asymptotically track a desired trajectory, i.e., time varying 4-DoF image geometric feature vector $\mathfrak{f}_d$.

We assume the perspective projection matrix is known. The control law is given as follows

$$\mathbf{v} = \mathbf{J}^{-1}\left(\dot{\mathfrak{f}}_d - \mathbf{K}\Delta\mathfrak{f}\right) \tag{21}$$

where $\mathbf{K}$ is a positive definite gain matrix and $\Delta\mathfrak{f} = \mathfrak{f} - \mathfrak{f}_d$.

Substituting (21) into (19) yields the closed-loop system

$$\Delta\dot{\mathfrak{f}} = -\mathbf{K}\Delta\mathfrak{f} \tag{22}$$

which is a linear time invariant autonomous system. Therefore, the system is asymptotically stable.

V. Experiments

A. Setup

The experiment setup consists of a first generation da Vinci Surgical System which provides three patient side manipulators (PSMs), one Endoscopic Camera Manipulator (ECM) on the patient side, and two master tool manipulators (MTMs) for teleoperation on the master side. The manipulators are controlled by the dVRK electronics and cisst/SAW software environment [24]. We mounted the stereo endoscope (only one channel used) on the ECM to get the image feedback, see Fig. 4. For simulating the scenario of minimally invasive surgery, we inserted the ECM and PSM into the torso model and adjusted the poses of them to guarantee that the tool is in the field of view of the endoscope by moving setup joints (SUJs), i.e., passive joints for holding the active arms. The OpenCV libraries were used to process the captured images.

B. Illuminance Varying Experiment

In this experiment, we quantitatively evaluated the robustness of our vision algorithm under different light illuminance as well as different robot positions. Meanwhile, we evaluated how accurate and precise the RCM projection estimation is using the data we collected under different robot positions.

We moved the robot to 20 different positions. For each position, we changed the intensity of the light source from 40% to 100% with the step of 20% of the full capacity. In this way, we collected 20 robot positions $\times$ 4 marker points $\times$ 4 light source intensities $= 320$ total measurements. For each image point $\mathbf{p}_{m_i}$ on the marker measured under the same robot position with 4 different light source intensities, we calculated the largest distance from those 4 image point measurements to their centroid. In total, we obtained 80 distances for all image points with different robot positions. The standard deviation and the mean value of those distances are 1.23 pixels and 1.49 pixels, respectively, which experimentally proves that our color scheme is effective and our segmentation algorithm is robust under different illuminance and different marker positions.

We repeated the experiment with the RCM in the field of view so that we can directly measure the projection of it as the ground truth. With the collected data, we obtained 20 lines for 20 robot positions. We calculated all the distances from the lines intersections to the ground truth (the measured projection of RCM) to evaluate the accuracy and precision of the estimation. The standard deviation and mean value of those distances are 2.13 pixels and 3.62 pixels, respectively. The experimental results prove that the estimation accuracy and precision are acceptable.

C. Pure Rotation Experiment

In this experiment, we commanded the robot to achieve pure rotations in the open loop with different initial positions. We did ten trials with the fourth joint initial position of the PSM varying from -3.5 rad to -1.25 rad with step 0.25 rad. Simultaneously, the algorithm computed the output of the rotation angles. The result of one trial, a comparison between the output of the algorithm and record of the robot encoder, is shown in Fig. 5. Although the computed angle has fluctuation, it generally matches the reference angle. Fig. 6 shows the error distribution of ten trials, in which the error is defined as the difference between the computed angle and the robot position. Mean values and standard deviations are listed in Table I. According to the experimental result, the median errors are around zero, most of the errors are smaller than 0.2 rad, and half of the errors are smaller than 0.1 rad.

D. Trajectory Tracking Experiment

In this experiment, we evaluated the implemented trajectory tracking controller. We planned the trajectory as $s_d =$

TABLE I
MEAN VALUES AND STANDARD DEVIATIONS OF ERRORS IN THE PURE ROTATION EXPERIMENT

Initial Position (rad)	-3.50	-3.25	-3.00	-2.75	-2.50	-2.25	-2.00	-1.75	-1.50	-1.25
μ (rad)	0.0232	0.0199	0.0110	0.0394	0.0219	-0.0073	-0.0062	-0.0030	0.0224	0.0273
σ (rad)	0.0916	0.0853	0.0768	0.0765	0.0778	0.0623	0.0579	0.0604	0.0579	0.0713

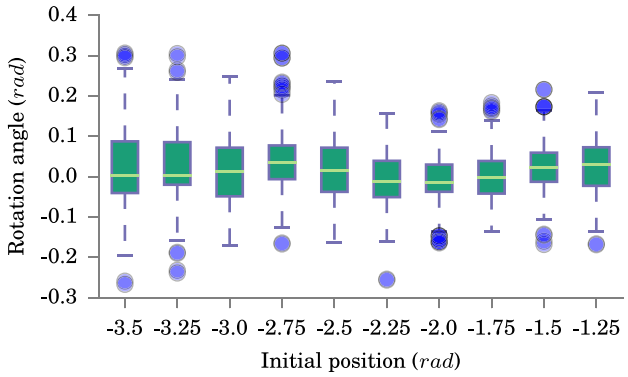

Fig. 6. The error distribution of ten trials.

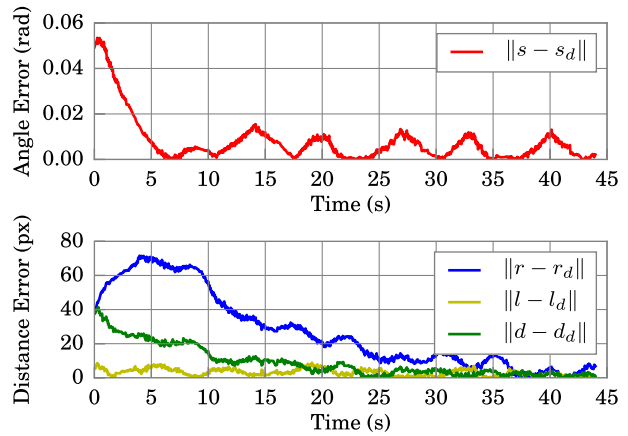

Fig. 7. The errors of the trajectory tracking experiment.

$A_s\sin(\omega t) + B_s$, $r_d = A_r\sin(\omega t) + B_r$, $s_l = A_l\sin(\omega t) + B_l$ and $d_d = A_d\sin(\omega t) + B_d$, where $\omega = 0.5$, $A_s = 0.05$, $B_s = 0.9$, $A_r = 60$, $B_r = 795$, $A_l = 30$, $B_l = 365$, $A_d = 37$ and $B_d = 212$. For the controller, we set the positive gain matrix K as a diagonal matrix with four gains $K_s = 0.032$, $K_r = 0.008$, $K_l = 0.0008$ and $K_d = 0.01$ on its diagonal. Since the experiment started in a random state, in which the current feature values are usually different from the desired feature values, some errors occurred during the initial stage. Fig. 7 shows that the errors converge to zero asymptotically, which experimentally proves that with the rotation distinguishing marker, the controller we implemented can fully control the 4 image degrees of freedom of laparoscopic instruments based on the image feedback of a monocular camera.

VI. CONCLUSION

In this letter, we have proposed a new method to fully control complete 4-image-DoF manipulation of laparoscopic instruments (with RCM mechanism) based on the geometric features of a designed marker in a 2D image. We designed the marker to encode the configuration of the instruments by computing geometric features among the projected image points from segmented areas in HSV space. We constructed an image geometric feature vector to locally characterize the configuration of a laparoscopic instrument. An image-based kinematic controller was introduced to asymptotically track a planned trajectory using the constructed feature vector as the feedback. We have evaluated our integration of rotation distinguishing marker and kinematic controller by several experiments in terms of illumination-invariance, rotation angle accuracy and controller performance. The presented experimental results show that our method can control the full 4 image degrees of freedom of RCM-constrained laparoscopic instruments, under different levels of illuminance with acceptable accuracy.

In the future, we plan to improve both the marker design and the computing algorithm so that the output of the rotation angle can be more stable and reliable. We will also explore methods to handle the occlusion caused by the blood stains by integrating occlusion handling algorithms.

REFERENCES

[1] J. Weerts *et al.*, "Laparoscopic nissen fundoplication: Detailed analysis of 132 patients," *Surg. Laparosc. Endosc. Percutan. Tech.*, vol. 3, no. 5, pp. 359–364, 1993.
[2] The COlon cancer Laparoscopic or Open Resection Study Group, "Laparoscopic surgery versus open surgery for colon cancer: Short-term outcomes of a randomised trial," *Lancet Oncol.*, vol. 6, no. 7, pp. 477–484, 2005.
[3] M. Braga *et al.*, "Training period in laparoscopic colorectal surgery," *Surgical Endoscopy Other Interventional Techn.*, vol. 16, no. 1, pp. 31–35, 2002.
[4] R. H. Taylor and D. Stoianovici, "Medical robotics in computer-integrated surgery," *IEEE Trans. Robot. Autom.*, vol. 19, no. 5, pp. 765–781, Oct. 2003.
[5] R. H. Taylor *et al.*, "A telerobotic assistant for laparoscopic surgery," *IEEE Eng. Med. Biol. Mag.*, vol. 14, no. 3, pp. 279–288, May/Jun. 1995.
[6] F. Alambeigi, R. J. Murphy, E. Basafa, R. H. Taylor, and M. Armand, "Control of the coupled motion of a 6 DOF robotic arm and a continuum manipulator for the treatment of pelvis osteolysis," in *Proc. IEEE Int. Conf. Eng. Med. Biol. Soc.*, 2014, pp. 6521–6525.
[7] F. Alambeigi, S. Behzadipour, G. Vossoughi, and F. Farahmand, "Simulation and control of a multi-dof laparoscopic tele-surgery system in virtual reality," in *Proc. 2011 2nd Int. Conf. Control, Instrum. Autom.*, 2011, pp. 1060–1066.
[8] D. Stoianovici *et al.*, "Endocavity ultrasound probe manipulators," *IEEE/ASME Trans. Mechatronics*, vol. 18, no. 3, pp. 914–921, Jun. 2013.
[9] A. R. Lanfranco *et al.*, "Robotic surgery: A current perspective," *Ann. Surg.*, vol. 239, no. 1, pp. 14–21, 2004.

[10] M. Azizian, M. Khoshnam, N. Najmaei, and R. Patel, "Visual servoing in medical robotics: A survey. Part i: Endoscopic and direct vision imaging-techniques and applications," *Int. J. Med. Robot.*, vol. 10, no. 3, pp. 263–274, 2014.

[11] F. Bourger, C. Doignon, P. Zanne, and M. De Mathelin, "A model-free vision-based robot control for minimally invasive surgery using ESM tracking and pixels color selection," in *Proc. IEEE Int. Conf. Robot. Autom*, 2007, pp. 3579–3584.

[12] D. R. Uecker, Y. Wang, C. Lee, and Y. Wang, "Laboratory investigation: Automated instrument tracking in robotically assisted laparoscopic surgery," *Comput. Aided Surg.*, vol. 1, no. 6, pp. 308–325, 1995.

[13] G.-Q. Wei, K. Arbter, and G. Hirzinger, "Real-time visual servoing for laparoscopic surgery. Controlling robot motion with color image segmentation," *IEEE Eng. Med. Biol. Mag.*, vol. 16, no. 1, pp. 40–45, Jan./Feb. 1997.

[14] A. Krupa *et al.*, "Autonomous 3-d positioning of surgical instruments in robotized laparoscopic surgery using visual servoing," *IEEE Trans. Robot. Autom.*, vol. 19, no. 5, pp. 842–853, Oct. 2003.

[15] M.-S. Kim, J.-S. Heo, and J.-J. Lee, "Visual tracking algorithm for laparoscopic robot surgery," in *Fuzzy Systems and Knowledge Discovery*. New York, NY, USA: Springer, 2005, pp. 344–351.

[16] S. Voros, G.-P. Haber, J.-F. Menudet, J.-A. Long, and P. Cinquin, "Viky robotic scope holder: Initial clinical experience and preliminary results using instrument tracking," *IEEE/ASME Trans. Mechatronics*, vol. 15, no. 6, pp. 879–886, Dec. 2010.

[17] J. Leven *et al.*, "DaVinci canvas: A telerobotic surgical system with integrated, robot-assisted, laparoscopic ultrasound capability," in *Proc. Int. Conf. Med. Image Comput. Comput. Assist Intervention*, 2005, pp. 811–818.

[18] J. Stoll, H. Ren, and P. E. Dupont, "Passive markers for tracking surgical instruments in real-time 3-D ultrasound imaging," *IEEE Trans. Med. Imag.*, vol. 31, no. 3, pp. 563–575, Mar. 2012.

[19] R. H. Taylor *et al.*, "Computer-integrated revision total hip replacement surgery: Concept and preliminary results," *Med. Image Anal.*, vol. 3, no. 3, pp. 301–319, 1999.

[20] T. Zhao, W. Zhao, D. Halabe, B. Hoffman, and W. Nowlin, "Fiducial marker design and detection for locating surgical instrument in images," Jul. 1, 2010, US Patent App. 12/428,657. [Online]. Available: https://www.google.com/patents/US20100168562

[21] D. Navarro-Alarcon, H. M. Yip, Z. Wang, Y.-h. Liu, W. Lin, and P. Li, "Adaptive image-based positioning of RCM mechanisms using angle and distance features," in *Proc. IEEE/RSJ Int. Conf. Intell. Robots Syst.*, 2015, pp. 5403–5409.

[22] F. Nageotte *et al.*, "Circular needle and needle-holder localization for computer-aided suturing in laparoscopic surgery," in *Proc. SPIE Med. Imag.*, 2005, pp. 87–98.

[23] F. Nageotte, P. Zanne, C. Doignon, and M. De Mathelin, "Visual servoing-based endoscopic path following for robot-assisted laparoscopic surgery," in *Proc. IEEE/RSJ Int. Conf. Intell. Robots Syst.*, 2006, pp. 2364–2369.

[24] P. Kazanzides *et al.*, "An open-source research kit for the da Vinci surgical system," in *Proc. IEEE Int. Conf. Robot. Autom*, 2014, pp. 6434–6439.

[25] D. A. Forsyth and J. Ponce, *Computer Vision: A Modern Approach*. Englewood Cliffs, NJ, USA: Prentice-Hall, 2002.

[26] N. Cazy, P.-B. Wieber, P. R. Giordano, and F. Chaumette, "Visual servoing when visual information is missing: Experimental comparison of visual feature prediction schemes," in *Proc. IEEE Int. Conf. Robot. Autom.*, 2015, pp. 6031–6036.

[27] G. Zhang, J. He, and X. Yang, "Calibrating camera radial distortion with cross-ratio invariability," *Opt. Laser Technol.*, vol. 35, no. 6, pp. 457–461, 2003.